EurJIC
European Journal of Inorganic Chemistry

A Journal of ChemPubSoc Europe

Accepted Article

Title: Molecular Engineering of Iridium Blue Emitters Using Aryl N-Heterocyclic Carbene Ligands

Authors: Mohammad Khaja Nazeeruddin; Sadig Aghazada; Aron Joel Huckaba; Antonio Pertegas Ojeda; Azin Babaei; Giulia Grancini; Iwan Zimmermann; Henk Bolink

To be cited as: Eur. J. Inorg. Chem. 10.1002/ejic.201600971

Link to VoR: http://dx.doi.org/10.1002/ejic.201600971

WILEY-VCH

FULL PAPER WILEY-VCH

Molecular Engineering of Iridium Blue Emitters Using Aryl N-Heterocyclic Carbene Ligands

Sadig Aghazada,[a] ‡ Aron J. Huckaba,[a]‡ Antonio Pertegas,[b] Azin Babaei,[b] Giulia Grancini,[b] Iwan Zimmermann,[a] Henk Bolink,[b] Mohammad Khaja Nazeeruddin,*[a]

Abstract: The synthesis of a new series of neutral Iridium (III) bis(2-(2',4'-difluorophenylpyridine)(1-(2'-aryl)-3-methylimidazol-2-ylidene) complexes is reported. Each complex has been characterized by NMR, UV-Vis, cyclic voltammetry, and the photophysical properties deeply explored. Furthermore, two of the complexes were characterized by single crystal X-ray diffraction. By systematically modifying the cyclometallating aryl group on the N-heterocyclic carbene (NHC) ligand from 2,4-dimethoxyphenyl to 4-methoxy-2-methyl-3-pyridine the energy levels of the Ir complexes were modified to produce new blue emitters with increased HOMO and triplet level energies. OLED devices fabricated with these emitters showed external quantum efficiencies (EQE) in the range of 2.3-3.2% with low turn-on values (2.7-2.9 V) and efficacies up to 6.3%..

Introduction

Reducing the energy consumption of light fixtures and display panels would significantly lower humanity's carbon footprint. Organic light emitting diodes (OLED) offer efficient illumination in a cost-effective manner, the performance of which has improved rapidly due to development of heavy atom emitters. Third row transition metals especially exhibit strong spin-orbit coupling (SOC), which allows fast intersystem crossing from excited singlet to triplet state and theoretical device efficiency near unity.[1,2] Among them, iridium is an excellent candidate for inclusion in OLEDs, due to its ability to emit at room temperature and its strong SOC that allows for efficient phosphorescence from its ^{3}MLCT state instead of the S_1 state.[3,4,5,6] Furthermore, Ir(III) complexes normally exhibit long (□s) excited-state lifetimes[5,7] and high photoluminescence quantum yields *(PLQY)*.[5,8]

Many Ir (III) emitters have been synthesized to date, but far fewer complexes have been shown to emit in the blue or violet region of the visible spectrum.[5] Since the first report of an isolable N-heterocyclic carbene (NHC) ligand, their use has spread far and wide.[9–12] Many cyclometallated Ir(III) complexes have also been reported.[13–15] Neutral [Ir(arylNHC)$_3$] complexes have been reported to exhibit high-energy emission with high *PLQY*.[16,17] Charged complexes have also been shown to exhibit high-energy emission upon excitation.[18–21] As for cyclometallated ligands in general, few homoleptic complexes have been reported as "true" blue emitters, with the few cases being mainly constrained to arylNHC or 2-arylimidazole complexes.[16,17,22–24] Heteroleptic complexes of the form (dfppy)$_2$Ir(L)[25–27] (where dfppy = 2-(2',4'-difluorophenyl)pyridine and L = a bidentate ligand) have been developed and explored as blue emitters, as have a range of fluorine free 2-(3'-pyridyl)pyridine-based emitters.[25,26,28,29] Blue emissive complexes of the structure (dfppy)$_2$Ir(L)$_2$, where L = isocyanide have also been very recently reported.[30]

The strong electron withdrawing nature of the dfppy ligand stabilizes the highest occupied molecular orbital (HOMO) much more than the lowest unoccupied molecular orbital (LUMO).[31] Such energy level tuning widens the HOMO-LUMO gap. As was thoroughly described by Zuo et al. very recently for the (dfppy)$_2$Ir(arylNHC) scaffold (and by others for other ligand classes),[31–33] the ancillary ligand also greatly impacts photophysical properties.[32] As a practical example, starting from (ppy)$_2$Ir(acac)[2] and changing the ancillary ligand can result in either a red-shift (as in 2,2'-bipyridine[34] or phenanthrene[35]) or blue-shift (as in (CN)$_2$[31,36] or bis(1-methylimidazol-3-yl-2-idene)methane, Im$_2$CH$_2$[18], or 2-picolinic acid)[37] of the observed

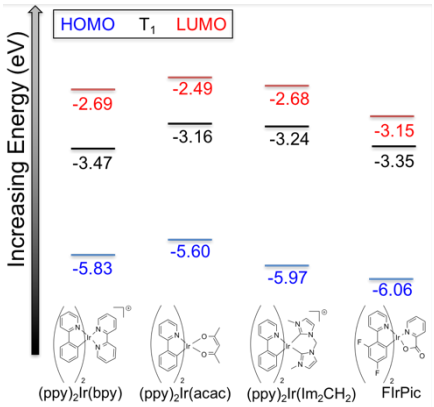

a:Group for Molecular Engineering of Functional Materials, Ecole Polytechnique Federale de Lausanne Valais Wallis, Rue de l'Indutrie 17, 1950 Sion, Valais, Switzerland E-mail: mdkhaja.nazeeruddin@epfl.ch

b: Instituto de Ciencia Molecular, Universidad de Valencia, c/Catedrático J. Beltrán, 2, 46980 Paterna, Spain

‡: These authors contributed equally.

Supporting information for this article is given via a link at the end of the document.

emission (Figure 1).

Figure 1. Illustration of ancillary ligand impact on emitter energy level position. HOMO and LUMO energy level values were taken from the respective references: $Ir(ppy)_2bpy$,[34] $Ir(ppy)_2acac$,[2] and $Ir(ppy)_2(Im_2CH_2)$,[18] FIrPic.[37] An estimate of the $E(T_1)$ value was made by the following conversion $E(T_1) = E_{(S+/S)} - (1240/\lambda_{em\ onset})$. $\lambda_{em\ onset}$ was estimated from the intercept of an emission curve tangent line with the baseline of the high energy side of the emission curve. Values in NHE obtained by converting first to SCE (Fc = 0.40 V vs SCE in 0.1 M NBu_4PF_6 MeCN) and then to NHE (SCE = 0.24 V vs NHE).[43] All NHE values converted to vacuum scale (fermi level of NHE = -4.5 eV vs vacuum).[38]

A recent study by Zuo et al. showed that by using progressively more withdrawn arylNHC ancillary ligands the emission energy could be increased to that of the sky blue FIrPic emitter by selective stabilization of the HOMO energy level[32] as is also the case for FIrPic.[27] Because of the success of Zuo et al., we sought to better understand the effect of NHC ancillary ligands bearing cyclometallating moieites with electron donating functionalities. In order to ascertain the influence of NHC ligand π-donor strength, the NHC ligands chosen were imidazole (**Ir1**-**Ir3**) or 1,2,4-triazole (**Ir4**). In order to better understand how the electron donating ability to both the Ir metal center and NHC ligand effects emission energy, aryl wingtip groups of different donating and accepting strengths were used as cyclometallating ligands (Figure 2).[6,17,18,32]

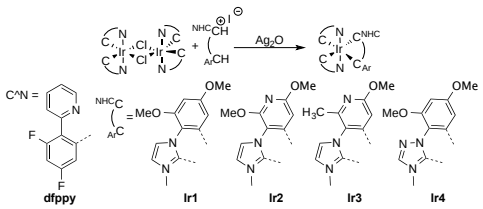

Figure 2. Structures of Neutral Iridium Complexes Used in this Study and the General Reaction to Reach Them.

Results and Discussion

Complex Synthesis

Each of the aryl NHC ligands was synthesized in two steps by Cu catalyzed coupling of the appropriate commercially available aryl bromide with imidazole or triazole,[39,40] followed by alkylation with methyl iodide (Scheme 1). The yields for the initial couplings were lower in this series than for aryls without methoxy substituents, likely due to reactant instability in the reaction conditions. One-pot metallation and subsequent transmetallation was achieved through reaction of each ligand with Ag_2O and $[(dfppy)_2IrCl]_2$.[16] Chromatographic separation and/or crystallization yielded each of the four complexes as a single isomer with the exception of **Ir4**.

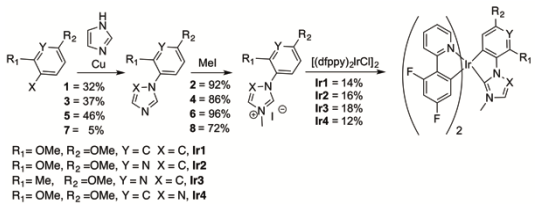

Scheme 1. Synthetic route to reach Ir complexes **Ir1**-**Ir4**.

*Crystal Structures of **Ir2** and **Ir3***

Single crystals of **Ir2** and **Ir3** were obtained either by vapor diffusion of hexanes into CH_2Cl_2 or concentration of a saturated $CDCl_3$ solution (See *Figure 3,* Supporting Information). Structures are shown in Figure 3, and other relevant structural data are listed in Tables S2, S3 of the Supporting Information. Both complexes exhibit a distorted octahedral geometry around the Ir center, with the pyridines *trans* to each other. All bonds involving Ir are > 2Å in length and the Ir-C4 (NHC) bond length is in the range 2.056-2.099 Å for both complexes. The Ir-NHC bond distance (Ir-C4, Table S2) is similar to those described for other Ir(III) NHC cyclometallated[14,17,18,32,34,41] and non-cyclometallated complexes.[42] The Ir-NHC is shorter in both cases than the Ir-Pyr bond, indicating a stronger bonding interaction.

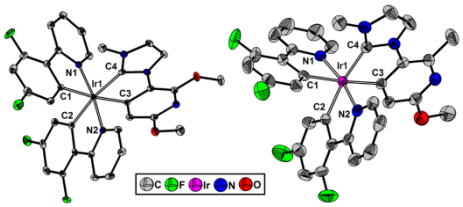

Figure 3. Drawings of complexes **Ir2** (left, measured at 100 K) and **Ir3** (right measured at 303 K) at 50% probability. Hydrogen atoms are omitted for clarity. Selected bond distances and angles shown in Tables S2, S3 in the Supporting Information.

Optical and Electronic Properties

Once the complexes were synthesized, they were characterized by cyclic voltammetry to better understand the structure-function relationship (see Table 1, Figure 4*a*). Upon obtaining oxidation and reduction potentials in 0.1M NBu_4PF_6 MeCN, we observed the ΔE_{red} for each of the complexes was nearly constant throughout the series and similar (+30 to -140 mV difference) to that observed for FIrPic. Instead of selectively modifying one energy level over the other, as was observed for the withdrawn arylNHC ligands,[32] both HOMO and LUMO levels were modified (Figure 4*b*). The complex with the highest ground state energy, (most destabilized HOMO, 1.14 V vs NHE) $E(S^+/S)$ value, was **Ir1** due to the dimethoxybenzene cyclometallating ligand and imidazole chelating group. The effect of σ-donation on $E(S^+/S)$ level is evidenced by the comparison of energy level values for **Ir1** and **Ir4**.

Table 1. Electrochemical Properties of complexes **Ir1**-**Ir4** and FIrPic.

Property	Ir1	Ir2	Ir3	Ir4	FIrPic
$E(S^+/S)^b$	1.14	1.24	1.24	1.43	1.56[d]

$E(S/S^-)^c$	-2.0(irr)	-2.0 (irr)	-2.0 (irr)	-1.64 (irr)	-1.65[d]
ΔE_{red}	3.14	3.24	3.24	3.07	3.21

a: Measured in a 0.1 M Bu_4NPF_6 in deoxygenated CH_3CN solution with glassy carbon working electrode, Pt wire reference and counter electrodes with Ferrocene/Ferrocenium (Fc/Fc^+) as an internal standard. $E^0(Fc^+/Fc)$ was taken as 0.64 V vs NHE and all values are converted and reported versus NHE.[43] b: $E(S^+/S)$ taken as $E_{(ox)} = 1/2(E_{pa} + E_{pc})$. c: Estimated from the peak of the irreversible reduction in reference to half wave potential of Fc^+/Fc; d: Taken from Ref. 37, originally reported in reference to (Fc/Fc^+) in 0.1M NBu_4PF_6 MeCN, converted to NHE by converting first to SCE (Fc = 0.40 V vs SCE in 0.1 M NBu_4PF_6 MeCN) and then to NHE (SCE = 0.24 V vs NHE).[43]

The less-donating triazole ligand contributed to stabilization of both $E(S^+/S)$ and $E(S/S^-)$ values. Furthermore, **Ir4** exhibited the most stabilized $E(S^+/S)$ value (1.43 V vs NHE). Substituting benzene with 3-pyridyl (complexes **Ir2** and **Ir3**) translated to a 100mV stabilization of the $E(S^+/S)$ energy level (1.24 V vs NHE) compared to **Ir1**, and substituting one methoxy for methyl on the pyridyl ring did not affect either the $E(S^+/S)$ or $E(S/S^-)$ energy level.

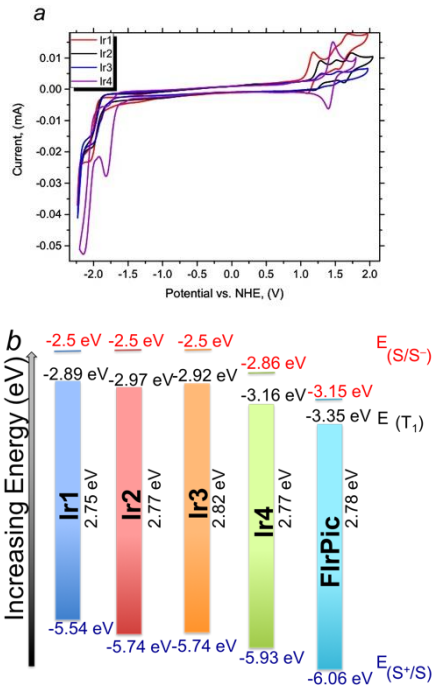

Figure 4. *a:* Cyclic voltammograms of complexes **Ir1** ("1", black), **Ir2** ("2", red), **Ir3** ("3", blue), **Ir4** ("4", teal) measured in 0.1 M NBu_4PF_6 CH_3CN solution. *b:* Energy level diagram of complexes **Ir1**-**Ir4**. $E(S^+/S)$ and $E(S/S^-)$ values obtained from CV in 0.1 M NBu_4PF_6 CH_3CN solution using Fc/Fc^+ as internal reference, Pt wire reference and counter electrodes, with glassy carbon disk working electrode. An estimate of the $E(T_1)$ value was made by the following conversion $E(T_1) = E_{(S+/S)} - (1240/\lambda_{em\ onset})$. $\lambda_{em\ onset}$ was estimated from the intercept of an emission curve tangent line with the baseline of the high energy side of the emission curve. Values for FIrPic taken from Ref. 37, originally reported in reference to (Fc/Fc^+) in 0.1M NBu_4PF_6 MeCN, values in NHE obtained by converting first to SCE (Fc = 0.40 V vs SCE in 0.1 M NBu_4PF_6 MeCN) and then to NHE (SCE = 0.24 V vs NHE).[43] All NHE values converted to vacuum scale (NHE = -4.5 eV vs vacuum).[38]

The photophysical behavior of the dissolved complexes has been observed by steady state and time resolved photoluminescence (PL) measurements in the sub-microsecond time window. The steady state PL spectra have been recorded in deoxygenated dichloroethane (DCE) by tuning the excitation wavelength to 375nm (Figure 6a). The most red-shifted emission was observed from **Ir1** (λ_{max} = 497 nm), while the most blue-shifted emission was observed from **Ir3** (λ_{max} = 464 nm). Taking the $\lambda_{em\ onset}$ (Figure 5, *vide infra*) as an estimate for the T_1 energy level, more conclusions can be drawn about the structure-function relationship between the different ancillary ligands. Changing the NHC from imidazole to triazole resulted in less energy lost between $E(S/S^-)$ and T_1 (300 mV for **Ir4** and 390 mV for **Ir1**). Surprisingly, while the HOMO and LUMO levels for **Ir2** and **Ir3** were identical, the emission energy was slightly different, with **Ir2** having a more stabilized $E(T_1)$ energy level.

The PL decay was registered at the PL maximum (see Table 2) for each of the complexes and Figure 6a shows the normalized PL spectra of the complexes synthesized along with the $Ir(ppy)_3$ as a reference. The PL dynamics are presented in Figure 6b. The complexes exhibit a mono-exponential decay in the sub-microsecond time window with similar time constant (τ_{PL}) of few hundreds of ns (see details in Table 2). From the retrieved constants, τ_{PL}, we could extract the radiative (k_{rad}) and non-radiative (k_{nrad}) rates according to the following equation:

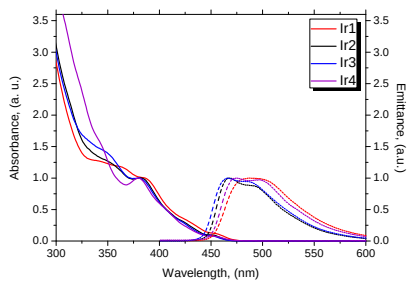

Figure 5. Normalized absorption (solid line) and emission (dashed line) Spectra for Complexes **Ir1** ("1", black), **Ir2** ("2", red), **Ir3** ("3", blue), **Ir4** ("4", teal) measured in deoxygenated DCE.

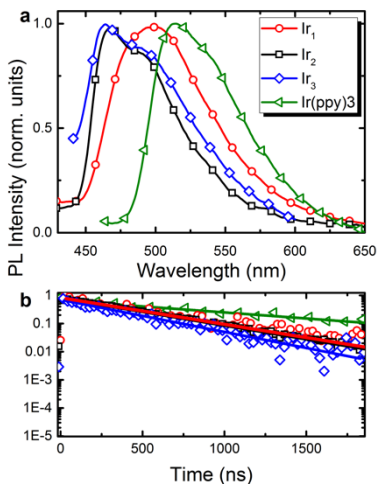

Figure 6 *a.* Photoluminescence spectra at 375 nm excitation for the samples indicated in the legend. *b.* PL time decay at 490 nm wavelength for the series as indicated in the legend of a. Solid lines represent the fits of the data (open symbols) obtained using a monoexponential function of the form y=A exp(-x/t). PL lifetimes obtained are listed in Table 2.

$$PLQY\ (\%) = k_{rad} / (k_{rad} + k_{nrad})$$

The *PLQY(%)* have been obtained comparing the measured PL spectra of each complex to the reference $Ir(ppy)_3$ having an established *PLQY* = 89% in deoxygenated DCE (see Supporting Information).[44] Considering that the PL lifetime is defined as the inverse of the sum of the rate constants of all the deactivating pathways of the excited states as $\tau_{PL} = 1/(k_{rad} + k_{nrad})$,[45] the rates were calculated and listed in Table 3. While the τ_{PL} constants were similar for each of the complexes, **Ir2** had the highest *PLQY* (0.66, Table 2) and **Ir3** displayed a lower *PLQY* (0.31, *PLQY*). Similarly, the k_{rad} value for **Ir2** was the highest (and k_{nrad} the lowest), with **Ir1** and **Ir2** having similar values for both (Table 2). The *PLQY* for complex **Ir4** was much lower than the rest (0.01 vs >0.31 for the others), likely because of quenching by isomeric impurities or by nonradiative processes. The extremely low observed *PLQY* also hindered τ_{PL} measurement. Unfortunately, this hypothesis could not be tested, as efforts to purify **Ir4** were not successful. The *PLQY* values observed are similar to those for other $(dfppy)_2Ir(ArNHC)$ complexes, however, the excited-state lifetimes we observed were substantially lower.[32] We calculated the Commission Internationale de l'Eclairage (CIE) coordinates for each of the emission spectra and observed that **Ir2** and **Ir3** displayed spectra that were modestly similar to the CIE coordinates for "Blue 476" of (0.1153,0.104) with values of (0.155,0.306) for **Ir2** and (0.157,0.294) for **Ir3** (Supporting Information).

Table 2. PL peak wavelength, *PLQY*, PL lifetime, calculated radiative (k_{rad}) and non-radiative (k_{nrad}) rates for **Ir1-Ir4**.

Property	Ir1	Ir2	Ir3	Ir4
PL Peak Wavelength (λ_p) (nm)	497	467	464	496
PLQY[a]	0.34	0.66	0.31	0.01
PL lifetime (τ_{PL}) (μs)	0.46	0.45	0.38	nd
k_{rad} ($10^6 s^{-1}$)	0.74	1.47	0.82	nd
k_{nrad} ($10^6 s^{-1}$)	1.43	0.75	1.81	nd
CIE Values (x,y)	0.187,0.430	0.155,0.306	0.157,0.294	0.174,0.380

a: Measurements taken in Ar saturated dichloroethane and compared against $Ir(ppy)_3$ to obtain a relative *PLQY* value. See Figure S2 in the supporting information for further details. b: Mixture of isomers (see Supporting Information).

OLED Device Characteristics

Because **Ir2** and **Ir3** exhibited the most blue-shifted emission spectra in solution, we chose to investigate their performance as OLED emitters. They were tested in the multilayer OLED shown in Figure 7b. S-P3MEET:PHOST (40 nm) acts as hole injection layer (HIL)[46] and XHT314 (20 nm) as hole transport layer (HTL) or electron blocking layer (EBL). The emissive layer (30 nm) (EML) was deposited from spin-coating using a host-guest system, where either **Ir2** (device 1) or **Ir3** (device 2) are dopants into TcTa (hole transport material) and OXD7 (electron transport material) cohost system. A thin layer of TSPO1 (10 nm) was thermally evaporated on top of the EML in order to efficiently confine excitons into the emissive layer, whereas a BmPymPb (40 nm) was evaporated as electron transport layer (ETM). Finally, Barium coated with silver was used as cathode. The OLED energy diagram is described in the Figure 7a. The energy levels reported were found in the literature.[47–50]

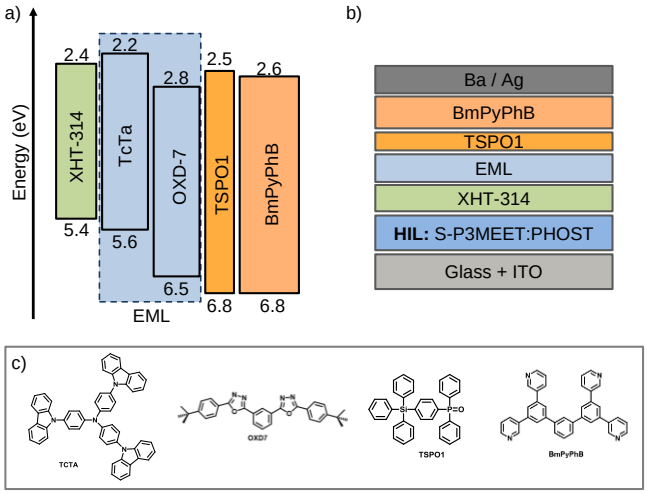

Figure 7. (a) Energy diagram and (b) device architecture for the OLEDs prepared using either **Ir2** or **Ir3** together with the (c) chemical structures of the emitting host materials and electron transport materials. The energy levels were obtained from the literature.

Figure 8 displays the OLED performance represented as the current density and luminance versus voltage (Figure 8a and b, respectively) and the efficacy and power efficiency versus luminance (Figure 8c and d, respectively). The current density profiles show typical diode behavior with a turn-on voltage around 3 volts. The profiles are very similar for the two OLEDs using the different emitting complexes. This implies that the charge transport is not significantly affected by the type of emitter used. In view of the similar device architecture and comparable energy levels of the two emitters, this is expected. The luminance starts at virtually the same turn-on voltage as the current density, yet for the OLED using complex 2 the luminance values are higher, which is in line with the higher *PLQY* observed for this complex. As a result, the efficacy (Figure 8c), power efficiency (Figure 8d) and external quantum efficiency are higher for the device 2, which achieved 8.0 cd A^{-1} (4.2 V), 6.3 lm W^{-1} (3.8 V) and 3.2% (4.2V) see Table 3.

Both OLEDs exhibit similar blue electroluminescence (EL) spectra (Figure 9) with a maximum peak at 489 nm and two shoulders at 471 nm and 530 nm. However, device 2 exhibits a more pronounced intensity for the second shoulder, which extends the EL spectrum to a slightly wider emission range. The CIE coordinates for the devices, therefore, are substantially further from "Blue 476" (0.1153,0.104) than devices incorporating FIrPic (0.18, 0.33),[51] with device 1 (0.238, 0.407) performing slightly better than device 2 (0.259, 0.409). The precise reason for the red-shifted shoulder (530 nm) is not known at this time. The highest energy peak observed in solution (467 nm for **Ir2** and 464 nm for **Ir3**) shifts to 471 nm and

takes on the appearance of a shoulder instead of a true peak upon inclusion in device EML. This shift is likely due to aggregation-based energy losses as evidenced by the difference in the device, drop-cast amorphous film, x-ray quality crystal, and solution emission spectra (Figure 9 and Figure S1 Supporting Information). In the solid state (amorphous film and crystal, Figure S1 Supporting Information), the peak is lost entirely and the highest energy transition is centered at 490 nm.

Figure 8. (a) J-V, (b) L-V, (c) Eff-V and (d) PE-V scan for the OLEDs containing either **Ir2** (red open circles) or **Ir3** (blue open squares).

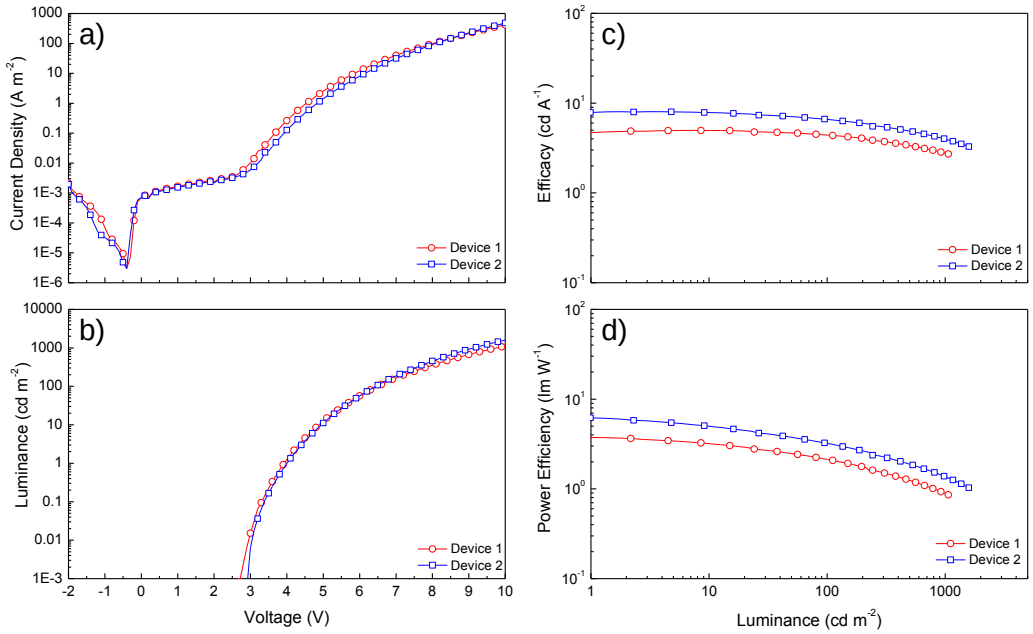

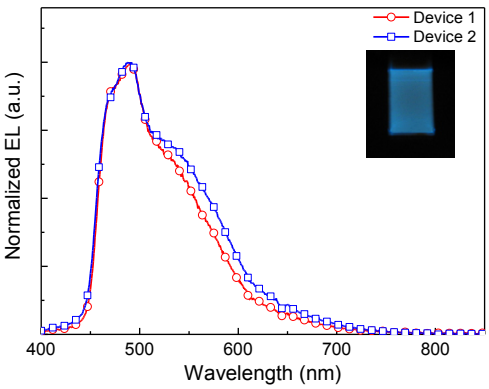

Figure 9. Electroluminescence spectrum for the OLEDs containing either **Ir2** (red open circles, device 1) or **Ir3** (blue open squares, device 2). Inset: Picture of the device 2.

Table 3. Device performance under J-V-L characterization of the OLEDs containing either **Ir2** or **Ir3** as emitters.

Device	Emitter	λ_{max} [nm]	CIE [x,y]	V_{on} [V]	Lum_{max} [cd m^{-2}]	$Efficacy_{max}$ [cd A^{-1}]	PE_{max} [lm W^{-1}]	EQE_{max} [%]
1	**Ir2**	489, 471(sh), 530(sh)	0.238, 0.407	2.7	1116	5.0	3.8	2.0
2	**Ir1**	489, 471(sh), 541(sh)	0.259, 0.408	2.9	1587	8.0	6.3	3.2

Conclusions

In the quest to lower energy consumption by developing more efficient ways to produce low-cost lighting, Ir (III) emitters are an attractive option. They are emissive ambient-air stable complexes capable of emitting at room temperature in many cases. Due to strong spin-orbit coupling, the complexes emit from a long-lived triplet state that enhances theoretical efficiency of OLED devices to near unity. Changing the ancillary ligand of the common Ir (III) complex $(dfppy)_2IrL$ from a weakly donating picolinate ligand to a strongly donating aryl NHC ligand allowed for the destabilization of the $E(S^+/S)$ and $E(T_1)$ value while maintaining a wide band-gap. Blue-emitting OLED devices were constructed utilizing the emitters and exhibited EQE up to 3.2% and turn on values as low as 3V.

Because the ancillary ligand plays such an important role in fine-tuning the photophysics of Ir (III) emissive complexes, judicious ligand selection is important to developing optimal emitters. Our future efforts into the development of new heteroleptic Ir (III) blue emitters will focus on proper "main"

ligand to "ancillary" ligand matching in order to most efficiently tune emission to higher energies.

Experimental Section

General Information: All commercially obtained reagents and OLED materials were used as received. Sulfonated poly{thiophene-3-[2-(2-methoxyethoxy)ethoxy]-2,5-diyl}:poly(4-hydroxystyrene) (SP3MEET:PHOST) and XHT314 (commercial crosslinkable hole transport material) were supplied by Solvay. *4,4',4''-Tris(carbazol-9-yl)triphenylamine* (TcTa), *1,3-Bis[2-(4-tert-butylphenyl)-1,3,4-oxadiazo-5-yl]benzene* (OXD-7), *Diphenyl-4-triphenylsilylphenyl-phosphine oxide* (TSPO1) and *1,3-Bis[3,5-di(pyridin-3-yl)phenyl]benzene* (BmPyPhB) were supplied by Luminescence technology Corporation (Lumtec). Unless otherwise noted, all reactions were performed under a N_2 atmosphere. Thin-layer chromatography (TLC) was conducted with Sigma T-6145 pre-coated TLC Silica gel 60 F_{254} aluminum sheets and/or visualized with UV and potassium permanganate staining. Flash column chromatography was performed as described by Still using Silicycle P60, 40-63 μm (230-400 mesh).[52] ^{1}H NMR spectra were recorded on a Bruker AVIII-HD (400 MHz), and are reported in ppm using solvent as an internal standard ($CDCl_3$ at 7.26 ppm). Data reported as: s = singlet, d = doublet, t = triplet, q = quartet, p = pentet, m = multiplet, b = broad, ap = apparent; coupling constant(s) in Hz; integration. UV-Vis spectra were measured with an LS-55 spectrometer. Cyclic voltammetry was measured with a Biologic S-200 cyclic voltammeter. Mass spectra were recorded on a Bruker Microflex MALDI-TOF or ESI mass spectrometer. IR were recorded on a Perkin Elmer UATR Two FT-IR spectrometer.

Photoluminescence (PL) Experimental Details: The time-resolved PL experiments were performed with a spectrophotometer (Gilden Photonics) coupled with a white lamp for steady state measurements or with the output of an optical parametric amplifier coupled with a Ti:sa picosecond laser (200 μm spot diameter, density of excitation around 30 μJ/cm2) and the signal was recorded at the selected wavelength using a Si-based photomultiplier detection technique with a time resolution of 1 ns.

Device Fabrication: The electroluminescent devices were prepared using patterned indium-tin-oxide (ITO) glass substrates sequentially cleaned with soap, de-ionized water, isopropanol and UV-O_3 lamp for 20 minutes. The hole injection layer (HIL), hole transport layer (HTL) and emissive layer (EML) were coated by spin-coating while the electron transport layer (ETL) and top electrode were thermally evaporated using an Edwards Auto500 evaporator integrated into a glovebox. The thickness of films was determined with an Ambios XP-1 profilometer. First, a 40 nm S-P3MEET:PHOST HIL was coated and annealed (180ºC) in air. Then, the substrates were transferred to inert atmosphere where XHT-314 HTL (20 nm) and the EML (30 nm) were coated from 1wt% toluene and chlorobenzene solution respectively. The emissive layer consisted of a mixture of TcTa, OXD-7 and the emitter at 10 wt% (solids). Subsequently, a thin 10 nm layer of TSPO1 and 40 nm ETL of BmPyPhB were thermally evaporated. Finally, the barium (5 nm) and silver (70nm) top electrode was thermally evaporated.

Device Characterization: The devices were characterized in an inert atmosphere without encapsulation. The current versus voltage (J-V) and luminance versus voltage (L-V) curves were obtained using a Keithley 2400 source meter and a photodiode coupled to a Keithley 6485 picoampmeter using a Minolta LS100 to calibrate the photocurrent. The electroluminescent spectra were measured using an Avantes AvaSpec-2048 Fiber Optic Spectrometer.

Synthetic Procedures to Reach Ir Emitters Ir1-Ir4:1-(2',4'-dimethoxyphenyl)imidazole (1).[19] An oven-dried Schlenk tube equipped with a stirring bar was charged with 1-bromo-2,4-dimethoxybenzene (2.2 g, 10 mmol), imidazole (0.95 g, 14 mmol), K_3PO_4 (4.24 g, 20 mmol). Anhydrous DMF (15 mL) was added and the mixture was deoxygenated with nitrogen for 20 minutes. Then CuI (0.38 mg, 2 mmol) was added and the reaction mixture was refluxed for 24 h. Afterward, the reaction was cooled down to room temperature, excess of dichloromethane was added and the mixture was washed with water. Organic phase was dried over $MgSO_4$, filtered and concentrated to a small amount. Flash chromatography on silica gel and with DCM:EtOAc (4:1) as eluent resulted in a pale yellow oil (650 mg, 32 %). ^{1}H NMR (400 MHz, Chloroform-*d*) δ 7.72 – 7.43 (broad signal, 1H), 7.25-6.28 (broad signal, 1H) overlapping with 6.98 (d, *J* = 8.6 Hz, 1H), 6.42 (d, *J* = 2.6 Hz, 1H), 6.34 (dd, *J* = 8.6, 2.6 Hz, 1H), 3.64 (s, 3H), 3.59 (s, 3H).

1-(2',4'-dimethoxyphenyl)-3-methylimidazolium iodide (2). In a round-bottom flask equipped with a stirring bar and condenser, 1 (0.64 g, 3.1 mmol) was dissolved in acetonitrile (20 mL). Then CH_3I (0.67 g, 4.7 mmol) was added and the reaction was refluxed for 12 hours. Afterwards, a product was precipitated with the excess of hexane and filtered. The pure product (0.99 g, 92 %) was obtained as white crystals after recrystallization from acetone:hexane. ^{1}H NMR (400 MHz, Acetonitrile-d_3) δ 9.50 (s, 1H), 7.84 (d, *J* = 1.8 Hz, 1H), 7.81 (d, *J* = 1.8 Hz, 1H), 7.55 (d, *J* = 8.7 Hz, 1H), 6.78 (d, *J* = 2.6 Hz, 1H), 6.64 (dd, *J* = 8.8, 2.5 Hz, 1H), 4.12 (s, 3H), 3.86 (s, 2H), 3.82 (s, 2H). IR (neat, cm^{-1}): 3105.3, 3083.1, 3056.2, 3006.8, 2987.8, 2946.4, 1611.1, 1555.7, 1503.6, 1295.1, 1211.6, 1035.2, 774.6, 614.7. HRMS (MALDI-TOF-MS): Theo. for $C_{12}H_{15}N_2O_2$, $[M]^+$:220.1212, observed: 220.143.

1-(2',6'-dimethoxy-3'-pyridine)imidazole (3). The synthetic procedure is analogous to the synthesis of 1-(2',4'-dimethoxyphenyl)-imidazole. 3-bromo-2,6-dimethoxypyridine (4.5 g, 20.6 mmol), imidazole (1.97 g, 29 mmol), K_3PO_4 (8.48 g, 40 mmol) and CuI (0.76 g, 4 mmol) in dry DMF (20 mL) were used. Flash chromatography on silica gel with acetone as eluent provided the product as a pale yellow oil (1.55 g, 37 %). ^{1}H NMR (400 MHz, Chloroform-*d*) δ 7.73 – 7.51 (broad signal, 1H), 7.36

(d, J = 8.2 Hz, 1H), 7.18 – 6.92 (broad signal, 2H), 6.26 (d, J = 8.2 Hz, 1H), 3.85 (s, 3H), 3.84 (s, 3H).

1-(2',6'-dimethoxy-3-pyridine)-3-methyl-imidazolium iodide (4). The synthetic procedure is analogous to the synthesis of 1-(2',4'-dimethoxyphenyl)-3-methylimidazolium iodide. 3 (1.46 g, 7.2 mmol), CH_3I (1.53 g, 10.8 mmol) and acetonitrile (30 mL) were used. Recrystallization from acetone-hexane afforded the product (2.15 g, 86 %) as a pale violet crystals. ^{1}H NMR (400 MHz, Acetonitrile-d_3) δ 8.90 (s, 1H), 7.81 (d, J = 8.5 Hz, 1H), 7.62 (d, J = 1.9 Hz, 1H), 7.55 (d, J = 1.8 Hz, 1H), 6.55 (d, J = 8.4 Hz, 1H), 4.04 (s, 3H), 4.01 (s, 3H), 3.97 (s, 3H). IR (neat, cm^{-1}): 3102.2, 3065.9, 3013.2, 2991, 1594.1, 1478.7, 1319.6, 1003.7, 816.6, 734.6. HRMS (MALDI-TOF-MS): Theo. for $C_{11}H_{14}N_3O_2$, $[M]^+$:221.1164, observed:221.132.

1-(6-methyl-2-methoxy-3-pyridine)imidazole (5). A flask equipped with a stirbar and reflux condenser was charged with imidazole (1.19 g, 17.44 mmol), K_2CO_3 (3.01 g, 21.8 mmol), 5-bromo-6-methyl-2-methoxypyridine (2.94 g, 2.0 mL, 14.5 mmol), CuO (0.29 g, 3.63 mmol), and DMSO (20 mL). The reaction mixture was then warmed to 150ºC open to air, allowed to stir, and monitored by ^{1}H NMR. After 16h, the reaction mixture was cooled to room temperature, diluted with CH_2Cl_2 (100 mL), the crude mixture passed through celite, washed with H_2O (3 x 50 mL), and dried with $MgSO_4$. Filtered, concentrated, and passed the crude mixture through an SiO_2 plug (75 mL) first using 20% CH_2Cl_2: Hexanes (0.56g of unreacted starting material in this fraction), CH_2Cl_2, and EtOAc (product in this fraction) to yield a pale orange solid (1.35 g, 46% yield). ^{1}H NMR (400 MHz, $CDCl_3$) δ 7.61 (bs, 1H), 7.40 (d, J = 8 Hz, 1H), 7.26 (bs, 1H), 7.04 (bs, 1H), 6.66 (d, J = 8 Hz, 1H), 3.97 (s, 3 H), 2.28 (s, 3H). ^{13}C NMR (100 MHz, $CDCl_3$) δ 163.1, 136.9, 129.8, 126.6, 108.5, 53.8, 20.3. IR (neat, cm^{-1}): 3117.0, 3098.2, 2988.8, 2941.9, 1580.3, 1499.1, 1474.7, 1301.3, 1030.35, 657.5. HRMS (ESI-MS): Theo. for $C_{10}H_{12}N_3O$, $[M]^+$: 190.0980, observed:190.0842. *1-(2'-methyl-6'-methoxypyridine)-3-methylimidazolium iodide (6)*. A flask equipped with a stirbar was charged with 1-(2'-methyl-4'-methoxy-3-pyridine)imidazole (0.50 g, 2.61 mmol), MeI (0.33 mL, 5.23 mmol), and MeCN (2 mL). The reaction mixture was then allowed to stir at 50ºC, and monitored by ^{1}H NMR. After 4h, the reaction mixture was concentrated, and recrystallized from CH_2Cl_2/Hexanes to yield an off-white solid (0.87 g, 96% yield). ^{1}H NMR (400 MHz, $CDCl_3$) δ 10.01 (bs, 1H), 7.90 (d, J = 8 Hz, 1H), 7.88-7.66 (m, 1H), 7.4-7.26 (m, 1H), 6.74 (d, J = 8 Hz, 1H), 4.31 (s, 3H) 4.00 (s, 3 H), 2.44 (s, 3H). ^{13}C NMR (100 MHz, *d_6-DMSO*) δ 163.9, 152.3, 138.5, 138.3, 125.1, 124.5, 124.3, 109.3, 54.4, 36.7, 20.3. IR (neat, cm^{-1}): 3117.0, 3098.2, 2988.8, 2941.9, 1580.3, 1499.1, 1474.7, 1301.3, 1030.35, 657.5. IR (neat, cm^{-1}): 3137.1, 3072.2, 2971.9, 1583.5, 1481.6, 1307.0, 812.5, 619.2. HRMS (ESI-MS): Theo. for $C_{11}H_{15}N_3O$, $[M-I]^+$: 215.1215, observed: 215.1500. *1-(2',4'-dimethoxyphenyl)-1,2,4-triazole (7).*[53] The synthetic procedure is analogous to the synthesis of 1-(2',4'-dimethoxyphenyl)imidazole. 1-iodo-2,6-dimethoxybenzene (2.5 g, 9.5 mmol, 1.2 equiv), 1,2,4-triazole (545 mg, 7.9 mmol, 1 equiv), K_3PO_4 (3.5 g, 16.6 mmol, 2.1 equiv) and CuI (75 mg, 0.4 mmol, 5 %) in dry DMF (15 mL) were used. Flash chromatography on silica gel with DCM - acetone (20 : 1) as eluent provided a product as a pale yellow oil (245 mg, 15 %). ^{1}H NMR (400 MHz, Chloroform-d) δ 8.60 (s, 1H), 8.06 (s, 1H), 7.59 (d, J = 8.5 Hz, 1H), 6.59 (m, 2H), 3.86 (s, 3H), 3.85 (s, 3H). *1-(2',4'-dimethoxyphenyl)-4-methyl1,2,4-triazol- iodide (8). 1-(2',4'-dimethoxyphenyl)-1,2,4-triazole* (245 mg, 1.2 mmol), CH_3I (400 mg, 2.8 mmol) and THF (4 mL) were mixed in high pressure flask equipped with a stirring bar. The flask was capped and mixture was heated to 105 ^{o}C for 3 hours. After 20 minutes a white precipitate formed. Afterwards, the mixture was cooled down, an excess of THF was added, a white precipitate filtered and washed with an excess of THF and dried under high vacuum (302 mg, 72 %). ^{1}H NMR (400 MHz, Acetonitrile-d_3) δ 9.94 (s, 1H), 8.76 (s, 1H), 7.73 (d, J = 8.9 Hz, 1H), 6.81 (d, J = 2.5 Hz, 1H), 6.73 (dd, J = 9.0, 2.5 Hz, 1H), 4.00 (s, 3H), 3.99 (s, 3H), 3.89 (s, 3H). HRMS (MALDI-TOF-MS) Theo. for $C_{11}H_{14}N_3O_2$, $[M]^+$:221.1164, observed: 221.151. *(2-(4',6'-difluorophen-2'-yl)pyridine)$_2$Ir(1-(4',6'-dimethoxyphen-2'-ylene)-3-methyl-imidazol-2-ylidene) (Ir1).* In an aluminium foil protected 25 mL round bottom flask equipped with a stirring bar $[(dfppy)_2IrCl]_2$ (0.2 g, 0.16 mmol) and 1-(2,4-dimethoxyphenyl)-3-methyl-1H-imidazol-3-ium iodide (0.12 g, 0.35 mmol) were dissolved in dichloroethane (15 mL). The solution was deoxygenated with nitrogen for 20 minutes and then Ag_2O (0.11 g, 0.49 mmol) was added and the flask was sealed with a stopper and electrical tape. The reaction mixture was stirred at reflux for 18 hours and then hot-filtered through celite. The filtrate was concentrated and purified by column chromatography on silica gel and with hexane:dichloromethane (1:3) as eluent. The product (40 mg, 14 %) was obtained as a yellow powder. ^{1}H NMR (400 MHz, Chloroform-d) δ 8.27 – 8.12 (m, 3H), 8.08 (d, J = 5.9 Hz, 1H), 7.78 (d, J = 5.2 Hz, 1H), 7.55 (dt, J = 16.8, 7.7 Hz, 2H), 6.79 – 6.67 (m, 2H), 6.66 (d, J = 1.9 Hz, 1H), 6.36 (dtd, J = 11.7, 9.2, 2.4 Hz, 2H), 6.17 (d, J = 2.5 Hz, 1H), 6.06 (dd, J = 7.9, 2.4 Hz, 1H), 5.98 (d, J = 2.4 Hz, 1H), 5.77 (dd, J = 8.5, 2.4 Hz, 1H), 3.90 (s, 3H), 3.56 (s, 3H), 3.15 (s, 3H). ^{19}F NMR (376 MHz, Chloroform-d) δ -110.03 (q, J = 9.1 Hz), -110.40 (q, J = 9.0 Hz), -110.81 (ddd, J = 12.1, 9.2, 2.8 Hz), -111.59 (ddd, J = 12.7, 9.4, 2.8 Hz). HRMS (ESI-MS): Theo. for $C_{34}H_{26}F_4IrN_4O_2$, $[MH]^+$: 791.1621, observed: 791.0087. *(2-(4',6'-difluorophen-2'-yl)pyridine)$_2$Ir(1-(2,6-dimethoxypyridin-3-yl)-3-methyl-1H-imidazol-3-ium) (Ir2).* The synthetic procedure analogous for *((2-(4',6'-difluorophen-2'-yl)pyridine)$_2$Ir(1-(4',6'-dimethoxy-5'-pyridin-2'-ylene)-3-methyl-imidazol-2-ylidene)* was carried out. $[(dfppy)_2IrCl]_2$ (0.4 g, 0.33 mmol), *1-(2',6'-dimethoxypyridin-3'-yl)-3-methylimidazolium iodide* (0.24 g, 0.69 mmol) and Ag_2O (0.23 g, 0.98 mmol) in dichloroethane (15 mL) were used. Column chromatography on silica gel with hexane:DCM (1:2) as eluent afforded the product as a yellow powder (95 mg, 16 %). ^{1}H NMR (400 MHz, Chloroform-d) δ 8.26 – 8.14 (m, 2H), 8.10 (t, J = 1.4 Hz, 1H), 8.06 (d, J = 5.9 Hz, 1H), 7.72 (d, J = 5.9 Hz, 1H), 7.57 (dt, J = 16.0, 7.9 Hz, 2H), 6.78 – 6.70 (m, 2H), 6.69 (s, 1H), 6.45 – 6.28 (m, 2H), 6.05 (dd, J = 8.0, 2.3 Hz, 1H), 5.85 (d, J = 1.0 Hz, 1H), 5.73 (dd, J = 8.5, 2.3 Hz, 1H), 4.04 (s, 3H), 3.76 (s, 3H), 3.15 (s, 3H). ^{19}F NMR (376 MHz, Chloroform-d) δ -109.52 (q, J = 9.0 Hz), -110.07 (q, J = 9.1 Hz), -110.62 (ddd, J = 12.6, 9.5, 2.8 Hz), -111.14 (ddd, J = 12.7, 9.6, 2.9 Hz). HRMS (ESI-MS): Theo. for $C_{33}H_{25}F_4IrN_5O_2$, $[MH]^+$: 792.1574, observed: 792.0132. *(2-(4',6'-difluorophen-2'-yl)pyridine)$_2$Ir(1-(6'-methyl-4'-methoxy-*

5'-pyridin-2'-yl)-3-methylimidazol-2-ylidene) (Ir3). A flask equipped with a stirbar was charged with 6 (0.15 g, 0.45 mmol), and 2-ethoxyethanol (5 mL). After degassing by vigorous N_2 sparging for 15 min $[(dfppy)_2IrCl]_2$ (0.25 g, 0.21 mmol), Ag_2O (0.42 g, 1.80 mmol) added and the flask sealed with a stopper and electrical tape. The reaction mixture allowed to stir at 120ºC, and monitored by ^{1}H NMR. After 18h, the reaction mixture was concentrated, suspended in CH_2Cl_2 (100 mL), passed through celite, and concentrated. The crude product was submitted to flash chromatography using a long SiO_2 column (700 mL), gradient of solvents from 33% CH_2Cl_2 : Hexanes with increasing polarity to 100% CH_2Cl_2 and continuing with increasing polarity to 100% EtOAc. The product was isolated as a 3:1 mixture of isomers (0.090 g, 18% yield). Selected key NMR data for the mixture: ^{1}H NMR (400 MHz, $CDCl_3$) δ *Minor isomer*: 8.31 (d, *J* = 8 Hz, 1H) 7.91 (d, *J* = 7.5 Hz, 1H), 7.31 (d, *J* = 8 Hz, 1H), 3.13 (s, 3H), 2.73 (s, 3H). *Major isomer*: 8.26-8.16 (m, *J* = 8 Hz, 2H) 8.01 (d, *J* = 7.5 Hz, 1H), 7.76 (s, 1H), 3.17 (s, 3H), 2.75 (s, 3H). ^{19}F {^{1}H} NMR (376 MHz, Chloroform-*d*) δ -109.46 (d, *J* = 9.1 Hz), -109.76 (d, *J* = 9.2 Hz), -110.03 (d, *J* = 9.3 Hz), -110.74 (d, *J* = 9.3 Hz). Single isomers were obtained after repetitive crystallization. HRMS (ESI-MS): Theo. for $C_{33}H_{24}F_4IrN_5O$, $[MH]^+$:775.1546, observed: 775.0011.

Alternate synthesis of Ir3: A flask equipped with a stirbar was charged with 5-(3'-methylimidazolium-1'-yl)-6-methyl-2-methoxypyridine iodide (0.25 g, 0.79 mmol), and chlorobenzene (50 mL). After degassing by vigorous N_2 sparging for 15 min, Ag_2O (0.18 g, 0.79 mmol), NEt_3 (0.12 mL, 0.79 mmol), $[(dfppy)_2IrCl]_2$ (0.44 g, 0.36 mmol), Ag_2O (0.42 g, 1.80 mmol) added, and a reflux condenser attached. The reaction mixture was allowed to stir at reflux, and monitored by ^{1}H NMR. After 18h, the reaction mixture was concentrated and submitted directly to flash chromatography using a long SiO_2 column (700 mL), gradient of solvents starting from CH_2Cl_2 with increasing polarity to 10% acetone: CH_2Cl_2. The product was isolated as a >15:1 mixture of isomers (0.40 g, 72% yield). analytical data identical to that of the above isolated Ir3. *(2-(4',6'-difluorophen-2'-yl)pyridine)$_2$Ir(1-(4',6'-dimethoxyphen-2'-yl)-4-methyltriazol-2-ylidene) (Ir4).* The synthetic procedure was analogous to that of (*(2-(4',6'-difluorophen-2'-yl)pyridine)$_2$Ir(1-(4',6'-dimethoxyphen-2'-yl)-3-methylimidazol-2-ylidene)*. $[(dfppy)_2IrCl]_2$ (0.3 g, 0.25 mmol), 1-(2',4'-dimethoxyphenyl)-4-methyltriazolium iodide (0.19 g, 0.54 mmol) and Ag_2O (0.17 g, 0.74 mmol) in dichloroethane (15 mL) were used. Column chromatography on silica gel with DCM:EtOAc (4:1) as eluent afforded the product as a yellow powder (55 mg, 14 %). Selected key NMR data for the mixture: ^{1}H NMR (400 MHz, Chloroform-*d*) δ for major isomer 9.64 (dd, *J* = 6.1, 1.5 Hz, 1H), 8.60 (d, *J* = 5.8 Hz, 1H), 8.30 (d, *J* = 8.5 Hz, 1H), 8.07 (s, 1H), 8.03 – 7.98 (m, 1H), 5.40 (dd, *J* = 9.6, 2.3 Hz, 1H), 5.13 (dd, *J* = 8.4, 2.3 Hz, 1H), 4.29 (s, 3H), 3.77 (s, 3H), 3.37 (s, 3H); and for minor isomer 9.58 (d, *J* = 5.9 Hz, 1H), 8.67 (d, *J* = 5.8 Hz, 1H), 7.64 (t, *J* = 7.8 Hz, 1H), 7.06 (t, *J* = 6.7 Hz, 1H), 5.65 (dd, *J* = 9.4, 2.3 Hz, 1H), 4.96 (dd, *J* = 8.6, 2.3 Hz, 1H), 4.29 (s, 3H), 3.77 (s, 3H), 3.25 (s, 3H). HRMS (ESI-MS): Theo. for $C_{33}H_{25}F_4IrN_5O_2$, $[M+H]^+$: 792.1574, observed: 792.0132.

Acknowledgements

This work was supported by the Swiss Federal Office for Energy (Energy program fund 563074 managed by Prof. Andreas Züttel) and the European Commission H2020-ICT-2014-1, SOLEDLIGHT project, grant agreement N°: 643791 and the Swiss State Secretariat for Education, Research and Innovation (SERI). We thank Prof. Hubert Girault for providing laser facilities. This work was supported by the Spanish Ministry of Economy and Competitiveness (MINECO) (MAT2014-55200 and MDM-2015-0538) and the Generalitat Valenciana (Prometeo/2012/053). We also thank Solvay OLED/Plextronics by provide the hole injection material and the hole transport material.

Keywords: Emissive Materials • Ir Complexes • Blue Emitters • OLED emitters • Phosphorescent Materials

(1) Baldo, M. A.; Lamansky, S.; Burrows, P. E.; Thompson, M. E.; Forrest, S. R. *Appl. Phys. Lett.* **1999**, *4* (75).
(2) Adachi, C.; Baldo, M. A.; Thompson, M. E.; Forrest, S. R. *J. Appl. Phys.* **2001**, *90* (10), 5048.
(3) Yersin, H.; Rausch, A. F.; Czerwieniec, R.; Hofbeck, T.; Fischer, T. *Coord. Chem. Rev.* **2011**, *255* (21-22), 2622–2652.
(4) Baldo, M. A.; O'Brien, D. F.; Thompson, M. E.; Forrest, S. R. *Phys. Rev. B* **1999**, *60* (20), 422–428.
(5) Papi, K.; Zanoni, S.; Coppo, R. L.; Amaral, R. C. *Dalt. Trans.* **2015**, *44*, 14559–14573.
(6) Thompson, M. *MRS Bull.* **2007**, *32* (September), 694–701.
(7) Sprouse, S.; King, K. A.; Spellane, P. J.; Watts, R. J. *J. Am. Chem. Soc.* **1984**, *106* (22), 6647–6653.
(8) Sajoto, T.; Djurovich, P. I.; Tamayo, A. B.; Oxgaard, J.; Goddard, W. A.; Thompson, M. E. *J. Am. Chem. Soc.* **2009**, *131* (28), 9813–9822.
(9) Arduengo, A. J.; Harlow, R. L.; Kline, M. *J. Am. Chem. Soc.* **1991**, *113* (1), 361–363.
(10) Herrmann, W. A. *Synth. Methods Organomet. Inorg. Chem.* **2000**, *9*, 84.
(11) Herrmann, W. A. A. *Angew. Chemie (International ed.)* **2002**, *41* (8), 1290–1309.
(12) Hopkinson, M. N.; Richter, C.; Schedler, M.; Glorius, F. *Nature* **2014**, *510* (7506), 485–496.
(13) Zuo, W.; Braunstein, P. *Organometallics* **2011**, *31* (7), 2606–2615.
(14) Chung, L.-H.; Lo, H.-S.; Ng, S.-W.; Ma, D.-L.; Leung, C.-H.; Wong, C.-Y. *Sci. Rep.* **2015**, *5* (October), 15394.
(15) Bauer, E. B.; Andavan, G. T. S.; Hollis, T. K.; Rubio, R. J.; Cho, J.; Kuchenbeiser, G. R.; Helgert, T. R.; Letko, C. S.; Tham, F. S. *Org. Lett.* **2008**, *10* (6), 1175–1178.
(16) Lee, J.; Chen, H.-F.; Batagoda, T.; Coburn, C.; Djurovich, P. I.; Thompson, M. E.; Forrest, S. R. *Nat. Mater.* **2016**, *15*, 92–98.
(17) Sajoto, T.; Djurovich, P. I.; Tamayo, A.; Yousufuddin, M.; Bau, R.; Thompson, M. E.; Holmes, R. J.; Forrest, S. R. *Inorg. Chem.* **2005**, *44* (22), 7992–8003.
(18) Monti, F.; Kessler, F.; Delgado, M.; Frey, J.; Bazzanini, F.; Accorsi, G.; Armaroli, N.; Bolink, H. J.; Ort, E.; Scopelliti, R.; Nazeeruddin, K.; Baranoff, E. *Inorg. Chem.* **2013**, *52*, 10292–10305.
(19) Stringer, B. D.; Quan, L. M.; Barnard, P. J.; Wilson, D. J. D.; Hogan, C. F. *Organometallics* **2014**, *33* (18), 4860–4872.
(20) Barnard, P. J. *Dalt. Trans.* **2015**, *44*, 8564–8576.
(21) Lu, K.-Y.; Chou, H.-H.; Hsieh, C.-H.; Yang, Y.-H. O.; Tsai, H.-R.; Tsai, H.-Y.; Hsu, L.-C.; Chen, C.-Y.; Chen, I.-C.; Cheng, C.-H. *Adv. Mater.* **2011**, *23* (42), 4933–4937.
(22) Karatsu, T.; Takahashi, M.; Yagai, S.; Kitamura, A. *Inorg. Chem.* **2013**, *52*, 12338–12350.
(23) Zhuang, J.; Li, W.; Wu, W.; Song, M.; Su, W.; Zhou, M.; Cui, Z. *New J. Chem.* **2015**, *39* (1), 246–253.
(24) Klubek, K. P.; Dong, S.-C.; Liao, L.-S.; Tang, C. W.; Rothberg, L.

J. *Org. Electron.* **2014**, *15* (11), 3127–3136.
(25) Frey, J.; Curchod, B. F. E.; Scopelliti, R.; Tavernelli, I.; Rothlisberger, U.; Nazeeruddin, M. K.; Baranoff, E. *Dalton Trans.* **2014**, *43* (15), 5667–5679.
(26) Duan, T.; Chang, T.; Chi, Y.; Wang, J.; Chen, Z.; Hung, W.; Chen, C.; Lee, G. *Dalt. Trans.* **2015**, *44*, 14613–14624.
(27) Baranoff, E.; Curchod, B. F. E. *Dalt. Trans.* **2015**, *44* (18), 8318–8329.
(28) Cola, L. De. *Chem. Mater*. **2012**, *24*, 3684–3695.
(29) Online, V. A.; Lee, J.; Oh, H.; Kim, J.; Park, K.; Yook, K. S.; Lee, J. Y.; Kang, Y. *J. Mater. Chem. C* **2014**, *2*, 6040–6047.
(30) Maity, A.; Le, L. Q.; Zhu, Z.; Bao, J.; Teets, T. S. *Inorg. Chem.* **2016**, *55* (5), 2299–2308.
(31) Li, J.; Djurovich, P. I.; Alleyne, B. D.; Yousufuddin, M.; Ho, N. N.; Thomas, J. C.; Peters, J. C.; Bau, R.; Thompson, M. E. *Inorg. Chem.* **2005**, *44* (6), 1713–1727.
(32) Li, T.; Liang, X.; Zhou, L.; Wu, C.; Zhang, S.; Liu, X.; Lu, G.; Xue, L.; Zheng, Y.; Zuo, J. *Inorg. Chem.* **2015**, *54*, 161–173.
(33) You, Y.; Park, S. Y. *J. Am. Chem. Soc.* **2005**, *127* (36), 12438–12439.
(34) Monti, F.; La Placa, M. G. I.; Armaroli, N.; Scopelliti, R.; Grätzel, M.; Nazeeruddin, M. K.; Kessler, F. *Inorg. Chem.* **2015**, *54* (6), 3031–3042.
(35) Zanoni, K. P. S.; Kariyazaki, B. K.; Ito, A.; Brennaman, M. K.; Meyer, T. J.; Murakami Iha, N. Y. *Inorg. Chem.* **2014**, *53* (8), 4089–4099.
(36) Nazeeruddin, K.; Berner, D.; Rivier, S.; Zuppiroli, L. *J. Am. Chem. Soc.* **2003**, No. 16, 8790–8797.
(37) Baranoff, E.; Curchod, B. F. E.; Monti, F.; Steimer, F.; Accorsi, G.; Tavernelli, I.; Rothlisberger, U.; Scopelliti, R.; Grätzel, M.; Nazeeruddin, M. K. *Inorg. Chem.* **2012**, *51* (2), 799–811.
(38) Bockris, J. O. M.; Khan, S. U. M. *Surface Electrochemistry*, 1st ed.; Springer US: New York, 1993.
(39) Huckaba, A. J.; Sharpe, E. A.; Delcamp, J. H. *Inorg. Chem.* **2015**, *55* (2), 682–690.
(40) Huckaba, A. J.; Hollis, T. K.; Howell, T. O.; Valle, H. U.; Wu, Y. *Organometallics* **2013**, *32* (1), 63–69.
(41) Tennyson, A. G.; Rosen, E. L.; Collins, M. S.; Lynch, V. M.; Bielawski, C. W. **2009**, No. 16, 6924–6933.
(42) Rajaraman, A.; Sahoo, A. R.; Hild, F.; Fischmeister, C.; Achard, M.; Bruneau, C. **2015**, *1414617*.
(43) Connelly, N. G.; Geiger, W. E. *Chem. Rev*. **1996**, *96* (2), 877–910.
(44) Endo, A.; Suzuki, K.; Yoshihara, T.; Tobita, S.; Yahiro, M.; Adachi, C. *Chem. Phys. Lett.* **2008**, *460* (1-3), 155–157.
(45) Magde, D.; Wong, R.; Seybold, P. G. *Photochem. Photobiol.* **2002**, *75* (4), 327–334.
(46) Belaineh, D.; Png, R.-Q.; McGuiness, C. L.; Mathai, M.; Seshadri, V.; Ho, P. K. H. *Chem. Mater*. **2014**, *26* (16), 4724–4730.
(47) Mesta, M.; Carvelli, M.; de Vries, R. J.; van Eersel, H.; van der Holst, J. J. M.; Schober, M.; Furno, M.; Lüssem, B.; Leo, K.; Loebl, P.; Coehoorn, R.; Bobbert, P. A. *Nat Mater* **2013**, *12* (7), 652–658.
(48) Lee, D. R.; Lee, C. W.; Lee, J. Y. *J. Mater. Chem. C* **2014**, *2* (35), 7256–7263.
(49) Darmawan, N.; Yang, C.-H.; Mauro, M.; Frohlich, R.; De Cola, L.; Chang, C.-H.; Wu, Z.-J.; Tai, C.-W. *J. Mater. Chem. C* **2014**, *2* (14), 2569–2582.
(50) Xu, L.-J.; Zhang, X.; Wang, J.-Y.; Chen, Z.-N. *J. Mater. Chem. C* **2016**, *4* (9), 1787–1794.
(51) Mulder, C. L.; Celebi, K.; Milaninia, K. M.; Baldo, M. A. *Appl. Phys. Lett.* **2007**, *90* (21).
(52) Still, W. C.; Kahn, M.; Mitra, A. *J. Org. Chem.* **1978**, *43* (14), 2923–2925.
(53) Petrosyan, V. A.; Burasov, A. V. *Russ. Chem. Bull.* **2010**, *59* (3), 522–527.

10.1002/ejic.201600971

WILEY-VCH

Entry for the Table of Contents (Please choose one layout)

Layout 1:

FULL PAPER

Destabilized but not Diminished. N-Heterocyclic Carbenes (NHCs) were investigated as ancillary ligands in $Ir(dfppy)_2L$ complexes, where dfppy = 2-(2',4'-difluorophenyl)pyridine. By utilizing arylNHC ligands of different electron accepting and donating strengths, the energy levels of the celebrated FIrPic were destabilized while maintaining blue emission. Blue OLED devices incorporating these emitters showed efficiencies up to 3.2% and turn on voltages as low as 2.7V.

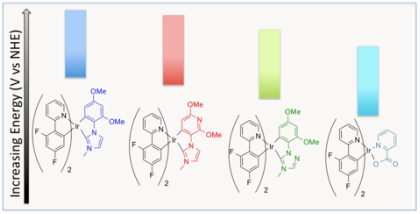

Sadig Aghazada,[a] ‡ Aron J. Huckaba,[a]‡ Antonio Pertegas,[b] Azin Babaei,[b] Giulia Grancini,[b] Iwan Zimmermann,[a] Henk Bolink,[b] Mohammad Khaja Nazeeruddin,[a]*

Molecular Engineering of Iridium Blue Emitters Using Aryl N-Heterocyclic Carbene Ligands